OXFORD

Human Molecular Genetics, 2015, Vol. 24, No. 15 4353–4364

doi: 10.1093/hmg/ddv168
Advance Access Publication Date: 10 May 2015
Original Article

ORIGINAL ARTICLE

Systemic AAV9 gene transfer in adult GM1 gangliosidosis mice reduces lysosomal storage in CNS and extends lifespan

Cara M. Weismann[1,2], Jennifer Ferreira[1,2], Allison M. Keeler[1,2], Qin Su[2], Linghua Qui[3], Scott A. Shaffer[4,5], Zuoshang Xu[3], Guangping Gao[2] and Miguel Sena-Esteves[1,2,*]

[1]Department of Neurology, [2]Gene Therapy Center, [3]Microbiology and Physiological Systems, [4]Biochemistry and Molecular Pharmacology and [5]Proteomics and Mass Spectrometry Facility, University of Massachusetts Medical School, Worcester, MA 01655, USA

*To whom correspondence should be addressed at: University of Massachusetts Medical School, 368 Plantation Street, ASC6-2055, Worcester, MA 01605, USA. Tel: +1 508 856 4412; Fax: +1 508 856 1552; Email: miguel.esteves@umassmed.edu

Abstract

GM1 gangliosidosis (GM1) is an autosomal recessive lysosomal storage disease where GLB1 gene mutations result in a reduction or absence of lysosomal acid β-galactosidase (βgal) activity. βgal deficiency leads to accumulation of GM1-ganglioside in the central nervous system (CNS). GM1 is characterized by progressive neurological decline resulting in generalized paralysis, extreme emaciation and death. In this study, we assessed the therapeutic efficacy of an adeno-associated virus (AAV) 9-mβgal vector infused systemically in adult GM1 mice ($\beta Gal^{-/-}$) at 1×10^{11} or 3×10^{11} vector genomes (vg). Biochemical analysis of AAV9-treated GM1 mice showed high βGal activity in liver and serum. Moderate βGal levels throughout CNS resulted in a 36–76% reduction in GM1-ganglioside content in the brain and 75–86% in the spinal cord. Histological analyses of the CNS of animals treated with 3×10^{11} vg dose revealed increased presence of βgal and clearance of lysosomal storage throughout cortex, hippocampus, brainstem and spinal cord. Storage reduction in these regions was accompanied by a marked decrease in astrogliosis. AAV9 treatment resulted in improved performance in multiple tests of motor function and behavior. Also the majority of GM1 mice in the 3×10^{11} vg cohort retained ambulation and rearing despite reaching the humane endpoint due to weight loss. Importantly, the median survival of AAV9 treatment groups (316–576 days) was significantly increased over controls (250–264 days). This study shows that moderate widespread expression of βgal in the CNS of GM1 gangliosidosis mice is sufficient to achieve significant biochemical impact with phenotypic amelioration and extension in lifespan.

Introduction

GM1 gangliosidosis is an autosomal recessive disorder resulting from mutations in the GLB1 gene encoding lysosomal acid β-galactosidase (βgal) (1). Mutations resulting in enzymatic deficiency lead to storage of a number of metabolites in the lysosomes. Namely, storage of GM1-ganglioside (GM1) and its asialo derivative GA1 occur primarily in the central nervous system (CNS) (2) while oligosaccharides and keratan sulfate accumulate in visceral organs (3). The incidence of GM1-gangliosidosis is estimated at 1 : 100 000–200 000 live births, but it is higher in certain ethnic groups and countries (4). GM1 patients are classified into three categories based on age of disease onset, which correlates to disease progression and severity of symptoms. The infantile form, which is the most aggressive of the three, is diagnosed in

Received: September 23, 2014. **Revised:** April 2, 2015. **Accepted:** May 5, 2015

the first 6 months of life and has the fastest progression with death occurring in <2 years (5). Late-infantile/juvenile form manifests between 3 and 36 months of age and continues for 1–5 years (5). The less common chronic/adult form has a wide range of onset from 3 to 30 years of age, and disease progression of 10–30 years (5). The age of onset is directly correlated with the residual activity of the mutant enzyme variants, with activity nearly absent in infantile-associated mutations, and up to 9% of normal in the adult forms (5). In infantile patients, the disease is characterized by rapid neurological decline, loss of voluntary motor control resulting in generalized paralysis, extreme emaciation and death. Other organs and tissues are also affected as evidenced by the characteristic hepatosplenomegaly and skeletal dysplasia. These clinical findings are either milder or absent in late-infantile and chronic forms of the disease where some residual enzyme activity is present. Currently, there is no treatment for GM1-gangliosidosis.

A number of gene therapy approaches have been tested in animal models of GM1-gangliosidosis, including *in vivo* infusion of adenovirus (6), adeno-associated virus (AAV) vectors (7–9), and *ex vivo* modification of autologous bone marrow stem cells with retrovirus vectors (10). The feasibility of these strategies is based on the ability of genetically modified endogenous cells, *in vivo* or *ex vivo*, to overexpress and release large quantities of functional lysosomal enzymes into the extracellular milieu. This secretion of enzyme allows for its distribution throughout the body via the blood stream. In the CNS, several mechanisms contribute to the distribution of lysosomal enzymes including the flow of cerebral spinal fluid (CSF) and interstitial fluid, as well as axonal transport (6,11,12). Most cells in the body are capable of taking up functional lysosomal enzymes and target them correctly to lysosomes via mannose-6-phosphate receptors on the cell surface (13). This uptake mechanism is the basis for enzyme replacement therapies (ERTs), hematopoietic stem cell transplantation, and gene therapy. ERT is the current standard of care for a number of lysosomal storage diseases affecting visceral organs. This is accomplished by regular parenteral infusion of recombinant enzymes. CSF infusion of recombinant enzyme is in clinical development for lysosomal storage diseases (LSDs) with neurological features (ClinicalTrials.gov: NCT01510028; NCT02055118). Direct infusion of AAV vectors into CSF or brain parenchyma has been the most effective *in vivo* gene delivery approach in animal models of GM1-gangliosidosis (7–9) and other LSDs with neurological features (14–16). The distribution of AAV vectors after intraparenchymal infusion is largely restricted to the injection site, although some AAV capsids also undergo axonal transport (17–19). One approach to achieve widespread distribution of enzymes throughout the CNS via axonal transport is to infuse AAV vectors into highly interconnected structures such as striatum (20,21), deep cerebellar nuclei (DCN) (22), ventral tegmental area (17), or thalamus (7). In mouse and cat models of GM1-gangliosidosis, the combination of bilateral thalamic and deep cerebellar injection of AAV vectors has proven exceptionally effective to correct lysosomal storage in the CNS (7,8). The therapeutic effect of this gene therapy approach in GM1 cats is remarkable with nearly complete correction of neurological symptoms and dramatic extension in their lifespan with restored reproductive capacity (8). Despite several CNS gene therapy clinical trials showing that intraparenchymal infusion of AAV vectors is well tolerated, it is still an invasive delivery approach (14,23,24).

AAV9 vectors are capable of crossing the blood–brain barrier (BBB) after intravascular delivery and achieve widespread transduction of neurons and glia in neonatal (25) and adult animals (25,26). This property of CNS transduction after vascular delivery appears to be a property shared by other AAV capsids (27,28). These new BBB-penetrating AAV vectors are attractive platforms to address the multi-systemic nature of most LSDs as they also transduce peripheral organs at high efficiency and thus have the potential to become whole body therapies with a single intravascular infusion. Systemic infusion of AAV9 vectors in adult mucopolysaccharidosis (MPS) IIIA (29) and IIIB (30) mice has proven highly effective in addressing lysosomal storage in the CNS and peripheral organs with resulting extension in lifespan. Interestingly in MPS VII mice it appears the biochemical alterations inherent to the disease compromise the therapeutic efficacy of AAV9 (31).

In the present study, we assessed the therapeutic efficacy of vascular administration of an AAV9 vector encoding mouse lysosomal βgal in adult GM1-gangliosidosis mice. A single administration of AAV9-βgal vector was sufficient to achieve enzyme expression and reduction of GM1-ganglioside content throughout the CNS. Most notably behavioral function remained stable longer and the lifespan was significantly increased in all AAV-treated cohorts.

Results

The therapeutic efficacy of systemic AAV9-βgal delivery was evaluated in adult GM1 mice ($\beta Gal^{-/-}$) infused with 1×10^{11} vg (low dose, LD, cohort; $N = 20$) or 3×10^{11} vg (high-dose, HD, cohort; $N = 34$) via the tail vein at 6 weeks of age (±2 days). This dose range was based on the first study demonstrating the therapeutic efficacy of an AAV9 vector administered systemically in adult MPS IIIB mice (30). Controls included phosphate-buffered saline (PBS)-injected GM1 mice ($N = 19$), and untreated age-matched normal heterozygote (HZ; $\beta Gal^{+/-}$) and wild-type (WT, $\beta Gal^{+/+}$) mice ($N = 49$). GM1 mice appear normal until ∼20 weeks of age when gait abnormalities and tremors become apparent. These mice reach the humane endpoint defined by >15% loss from maximum body weight or paralysis of any limb at ∼37 weeks of age. A subset of mice from AAV9-treated GM1 and control cohorts were euthanized at 37 weeks of age for histological and biochemical studies. Behavioral testing was performed at 10 and 30 weeks of age.

Partial restoration of βgal activity in CNS and overexpression in peripheral organs

Histochemical staining of brain sections revealed an increase in βgal activity throughout the brain of 37-week-old AAV-treated GM1 mice in the HD cohort (Fig. 1A, first and second rows) compared with PBS-treated GM1 mice (Fig. 1A, bottom row). Distribution of βgal activity appeared largely similar to that in the brain of HZ mice (Fig. 1A, third row). Biochemical quantification showed a significant increase in βgal activity throughout the CNS of AAV9-treated GM1 mice compared with age-matched PBS-injected GM1 mice (Fig. 1B and C; Supplementary Material, Table S1). βgal activity was dramatically elevated in liver, heart, muscle and serum of AAV9-treated GM1 male and female mice (Fig 1B and C; Supplementary Material, Table S1). The relative βgal activity (% WT) in cerebrum, cerebellum and brainstem of AAV9-treated GM1 mice was dose and sex dependent, and for the most part below normal levels. In peripheral tissues, relative βgal levels were considerably higher (Supplementary Material, Table S1). Liver βgal activity in the AAV-treated GM1 males and females at the humane endpoint was comparable with that at the 37 weeks of age (Supplementary Material, Fig. S1).

The vector genome content in CNS and peripheral organs was consistent with enzymatic findings, with the highest amounts in

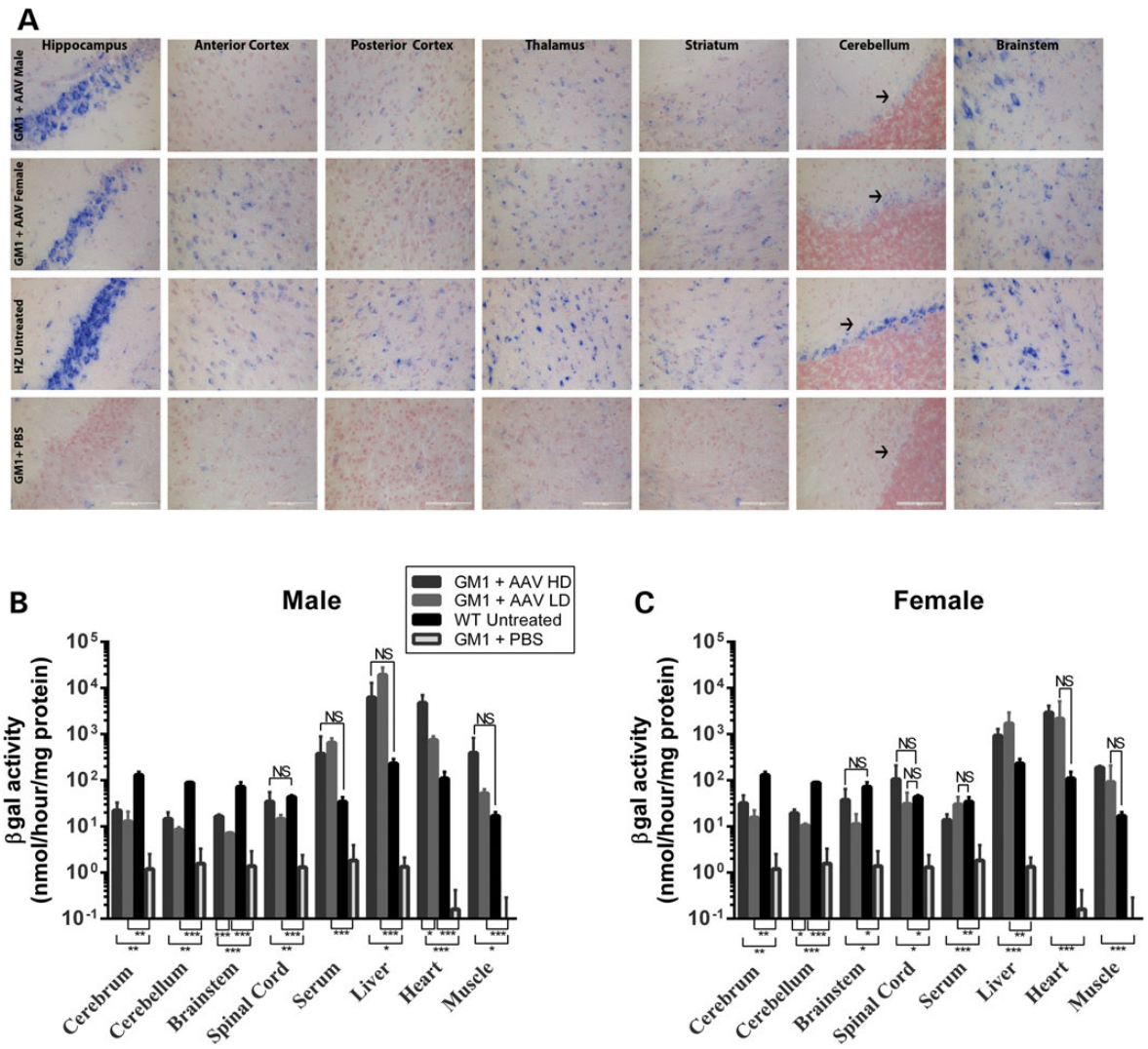

Figure 1 Increased βgal enzyme activity in AAV9-treated GM1 mice. (**A**) Xgal staining (blue) for βgal enzyme activity and counterstained with Nuclear Fast Red (red) at 37 weeks in different brain regions in representative AAV9-treated GM1 male and female mice in the HD cohort (3×10^{11} vg, GM1 + AAV), normal HZ, and control GM1 mice infused with PBS (GM1 + PBS). (**B** and **C**) Enzyme activity in CNS and peripheral tissues was determined by 4-MU assay at 37 weeks of age in (B) male or (C) female mice in the HD cohort (3×10^{11} vg) or LD cohort (1×10^{11} vg). Results are shown as mean ± SD, GM1 + AAV $N = 3$, WT or GM1 + PBS $N = 4$. * $P < 0.05$, ** $P < 0.01$ and *** $P < 0.001$, unpaired Student's *t*-test.

liver and the lowest in CNS of AAV-treated GM1 mice (Table 1). The vector genome content in the male liver was higher than in females (Table 1). An additional study revealed no significant effect of genotype or mouse strain on the biodistribution profile of the AAV9-βgal vector (Supplementary Material, Table S2).

Reduction of GM1-ganglioside content and reduction in astrogliosis throughout CNS

In GM1 mice and patients reduced βgal activity results in accumulation of GM1-ganglioside in the CNS. Previous work has shown that a filipin stain can be used to detect lysosomal storage in the brain of GM1 mice as it has been shown to bind cholesterol and the GM1-ganglioside (9,32). Filipin staining of normal brain appears as a diffuse blue signal distributed uniformly throughout with no defined cellular structures (data not shown), likely due to the normal membrane localization of cholesterol and GM1-ganglioside (9). In a filipin stained GM1 brain, storage appears as bright perinuclear puncta. Filipin staining of brain sections from AAV9-treated GM1 mice in the HD cohort at 37 weeks revealed partial correction of lysosomal storage in most brain regions (Fig. 2A). The impact on lysosomal storage appeared to be modest in thalamus, striatum and granule/Purkinje cell layers (thin arrows, Fig. 2A) in the cerebellum. Interestingly, we observed complete clearance of storage in DCN (Fig. 2A; thick arrows in top row and middle row). The reduction in lysosomal storage material in the brain was more pronounced in female than male mice (Fig. 2A, top and middle row). Similarly, in spinal cord, there was a dramatic reduction in storage in HD cohort females (Fig. 2B, third row), but variable response in males (Fig. 2B, top two rows). The impact on lysosomal storage in CNS was minimal in the low dose (LD) cohort (1×10^{11} vg) (Supplementary Material, Figs S2 and S3). In the HD cohort, GM1-ganglioside content was significantly reduced in the cerebrum, brainstem and spinal cord compared with PBS-injected GM1 mice at 37 weeks of age (Fig. 2C). In agreement with the histological analysis

Table 1. Vector genome content in CNS and peripheral tissues of AAV9-treated GM1 mice

Vector genome copies/diploid genome (mean ± SD)		
Tissue	Male	Female
Cerebrum	$6.39e^{-3} \pm 0.39e^{-3}$	$20.2e^{-3} \pm 9.84e^{-3}$
Cerebellum	$2.25e^{-3} \pm 0.52e^{-3}$	$4.94e^{-3} \pm 1.82e^{-3}$
Spinal cord	$5.52e^{-3} \pm 1.07e^{-3}$	$15.6e^{-3} \pm 14.3e^{-3}$
Liver	$36.5 \pm 7.91^{**}$	$6.81 \pm 2.14^{**}$
Heart	$4.36e^{-1} \pm 3.56e^{-1}$	$11.0e^{-1} \pm 2.19e^{-1}$
Muscle	$2.09e^{-1} \pm 1.83e^{-1}$	$1.49e^{-1} \pm 0.32e^{-1}$
Kidney	$9.82e^{-2} \pm 7.72e^{-2}$	$24.5e^{-2} \pm 14.1e^{-2}$
Spleen	$2.87e^{-2} \pm 1.85e^{-2}$	$6.15e^{-2} \pm 1.20e^{-2}$
Lung	$3.77e^{-2} \pm 0.63e^{-2*}$	$6.56e^{-2} \pm 0.87e^{-2*}$

Male and female GM1 mice in the HD cohort (3×10^{11} vg) were sacrificed at 20 weeks of age ($N = 3$ per group). Vector genome content was measured in 25–100 ng of genomic DNA from each tissue by Taqman real-time PCR.
*$P < 0.05$.
**$P < 0.01$, unpaired Student's *t*-test.

of storage distribution in brain by filipin staining, the GM1-ganglioside content in cerebrum was lower in females than males in the HD cohort ($P = 0.04$, Fig. 2C). The GM1-ganglioside content in cerebellum was not significantly changed by AAV9 treatment.

Astrogliosis was apparent throughout the CNS of PBS-treated GM1 controls (Fig. 3A and B, bottom rows), as shown previously in GM1 mice (33). High dose AAV9 treatment resulted in a marked decrease in reactive astrocytes across the cerebrum (Fig. 3A, first and second rows), but a more moderate impact in the striatum, especially in males (Fig. 3A, top row). The spinal cords of AAV9-treated GM1 mice of both genders were comparable with that of normal controls (Fig. 3B).

Dose- and gender-dependent behavioral performance

A number of tests were carried out at 10 and 30 weeks of age to assess motor performance and behavior over time (Fig. 4; Supplementary Material, Figs S4 and S5). In the rotarod test, 30-week-old AAV9-treated GM1 mice performed significantly better than

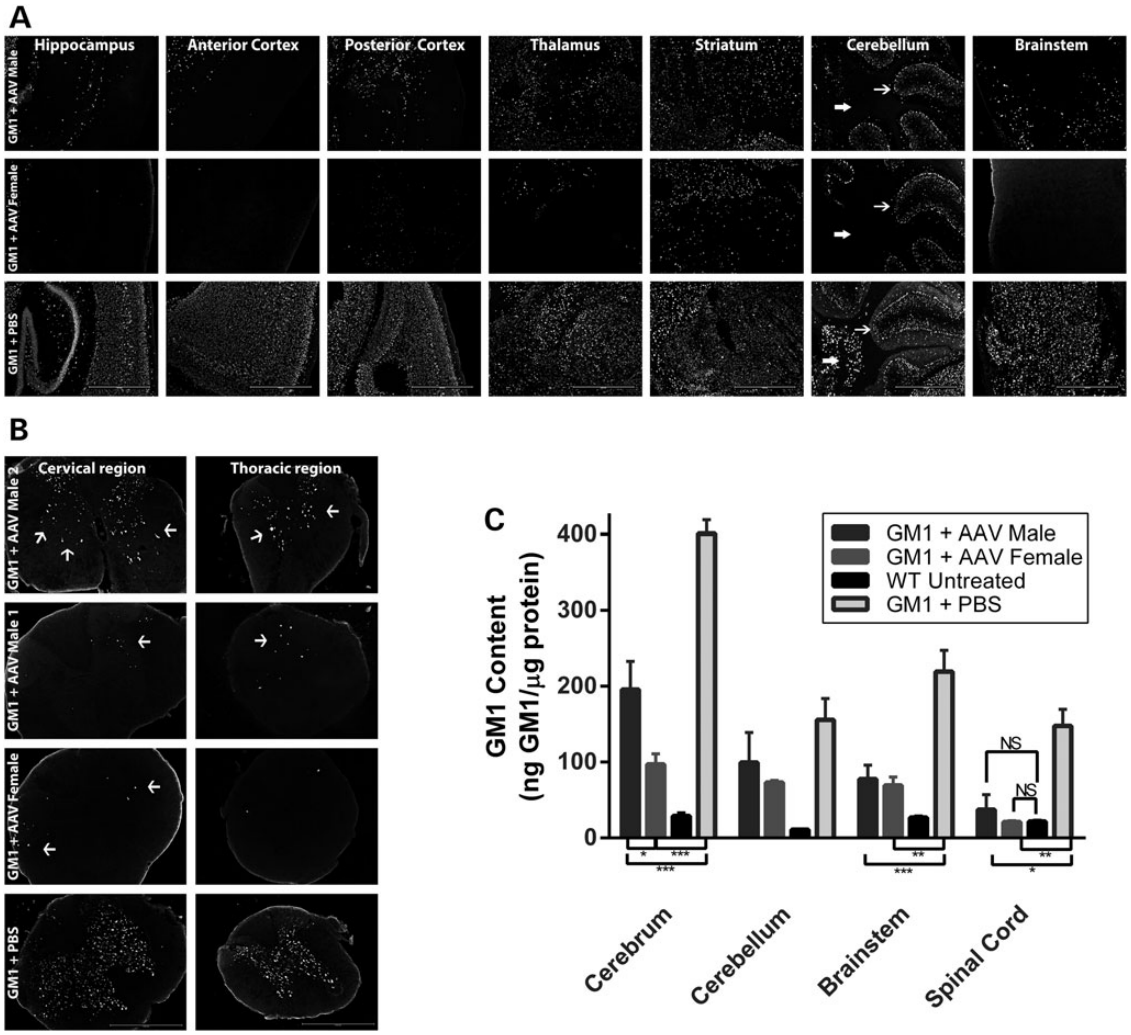

Figure 2. Lysosomal storage is reduced in the CNS of AAV9-treated GM1 mice. (**A**) Filipin staining of selected brain regions, and (**B**) filipin staining of cervical and thoracic region of spinal cord in 37 weeks old mice. Representative pictures from GM1 male and female mice treated with 3×10^{11} vg (HD) of AAV9-βgal vector (GM1 + AAV), or PBS (GM1 + PBS) are shown. Scale bar indicates 1 mm. Thin and thick white in (A) arrows indicate the Purkinje cell layer, and DCN, respectively. White arrows in (B) indicate Filipin staining in the spinal cord of AAV-treated animals. (**C**) GM1-ganglioside content in the CNS of the same cohorts measured by LC–MS/MS. Results are shown as mean ± SD. GM1 + AAV $N = 3$ (GM1 + AAV, female, $N = 2$). WT or GM1 + PBS $N = 4$. *$P < 0.05$, **$P < 0.01$ and ***$P < 0.001$, unpaired Student's *t* test. NS indicates non-significant differences.

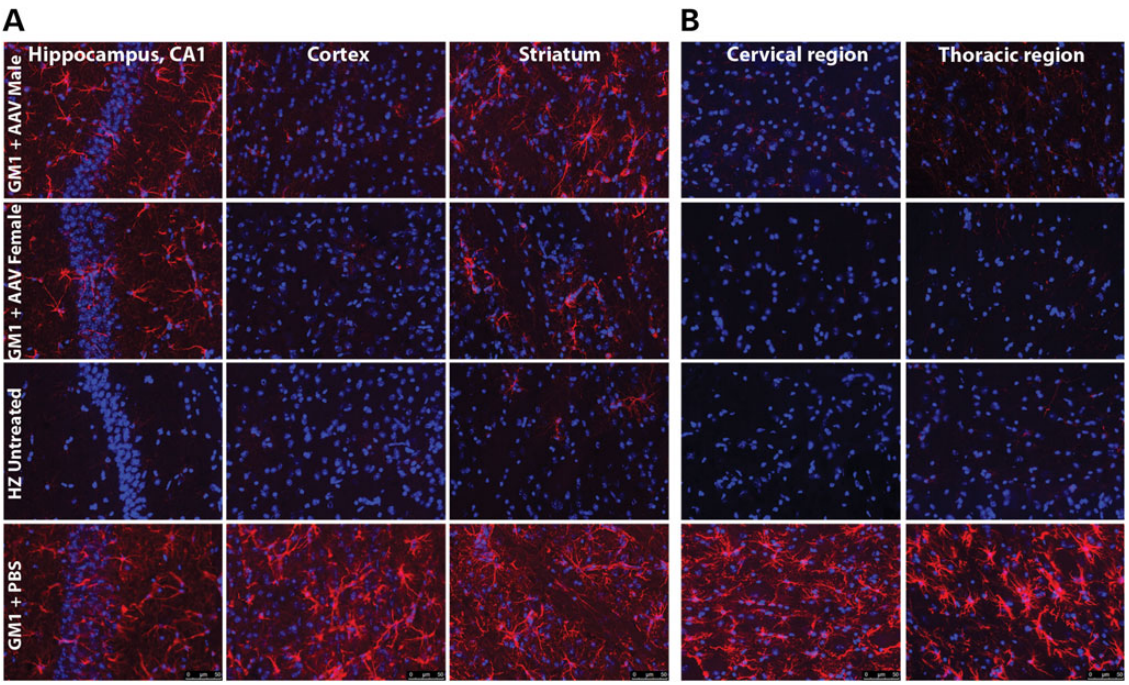

Figure 3. Astrocytosis in the CNS of GM1 mice is reduced by AAV9 vector treatment. (**A**) GFAP staining in the hippocampus, CA1 region, cortex and striatum, (**B**) cervical and thoracic spinal cord in representative male and female GM1 mice treated with 3×10^{11} vg (HD) of AAV9-βgal vector (GM1 + AAV), a normal HZ and PBS-treated GM1 mouse (GM1 + PBS) mice at 37 weeks of age. Scale bars indicate 50 μm.

age-matched PBS-treated GM1 mice, and were comparable with normal controls for most treatment cohorts (Fig. 4A and B). In the inverted screen test, AAV9-treated GM1 females in the HD cohort, but not the LD cohort, scored significantly better in both time on screen and number of hindlimb movements than PBS-treated females at 30 weeks of age (Fig. 4D and F). In contrast, only males in the LD cohort performed better than PBS-treated males in percentage of time on screen at 30 weeks of age (Fig. 4C).

Home cage testing captures a large number of behaviors of an animal in a familiar environment and can identify phenotypic alterations not detectable by traditional motor function testing (34). Animals were evaluated over a 24 h period that spans the 12 h light cycle when animals are less active (Fig. 4G and H, left graphs) and the 12 h dark cycle when animals are most active (Fig. 4G and H, right graphs). AAV9-treated GM1 males in HD and LD cohorts performed significantly better than PBS-treated GM1 males in vertical reaching in both periods (Fig. 4G) and in exploratory behavior during the day (Fig. 4G and left side). However, only the HD males performed significantly better than PBS controls in exploratory behavior during the night (Fig. 4G, right side). Females in HD and LD cohorts performed significantly better than PBS-treated females in daytime vertical movements and exploratory behavior (Fig. 4H, left side); however, only females in the HD cohort retained significantly better performance than PBS-treated controls in these measured behaviors during the nighttime (Fig. 4H, right side). Females in the HD cohort were able to hang from the overhead wire feed tray significantly better than PBS-treated control females in both light cycles (Fig. 4H).

Movies of animals moving freely were made at 220–260 days old to document phenotypes of AAV9-treated and untreated animals close to the median humane endpoint of untreated GM1 mice. In all videos with PBS-treated GM1 mice (Supplementary Material, Movies S1–S4), hallmark phenotypes of GM1 mice were noted as previously reported in this model (35,36). Whole body tremors and gait abnormalities were evident in these mice. The front legs were tucked under the torso but remained functional and the body was consistently tilted forward suggesting weakness in forelimbs or shoulder muscles. The hind legs were splayed outward but remained capable of supporting body weight. Interestingly, hind leg movement appeared to be initiated by hip rotation suggestive of quadriceps weakness, which may also be the cause for reduced rearing or vertical movements. Tail stiffness and curling over the body was also a common phenotype in these control mice as described in GM1 mice (36). AAV9-treated GM1 males in the HD cohort displayed some tail stiffness, but normal body position, mobility and rearing activity at 258 days (Supplementary Material, Movie S1). Male mice in the LD cohort at 263 days showed tail stiffness, unsteady gait and slight tremors, but rearing was still apparent during grooming (Supplementary Material, Movie S3). Female mice in the HD cohort at 260 days (Supplementary Material, Movie S2) were largely indistinguishable from normal controls. GM1 female mice in the LD cohort at 264 days (Supplementary Material, Movie S4) displayed some tremors, but body position was close to normal albeit lower to the ground, and gait abnormalities such as occasional hopping were milder than in PBS-treated GM1 mice at comparable age. Long lived GM1 females in the HD cohort remained ambulatory but displayed clear signs of decline with stiff tails, jerky movements, whole body tremors, and walking low to the ground at 590 days old (Supplementary Material, Movie S5) and 566 days old (Supplementary Material, Movie S6).

AAV treatment extends lifespan of βGal$^{-/-}$ mice

PBS-treated GM1 mice reached maximum weight at an average of 175 ± 21 days of age (>15% body weight loss from maximum) (Fig. 5A and B and Table 2). Maximum body weight of AAV9-treated GM1 mice was reached significantly later than PBS-treated GM1

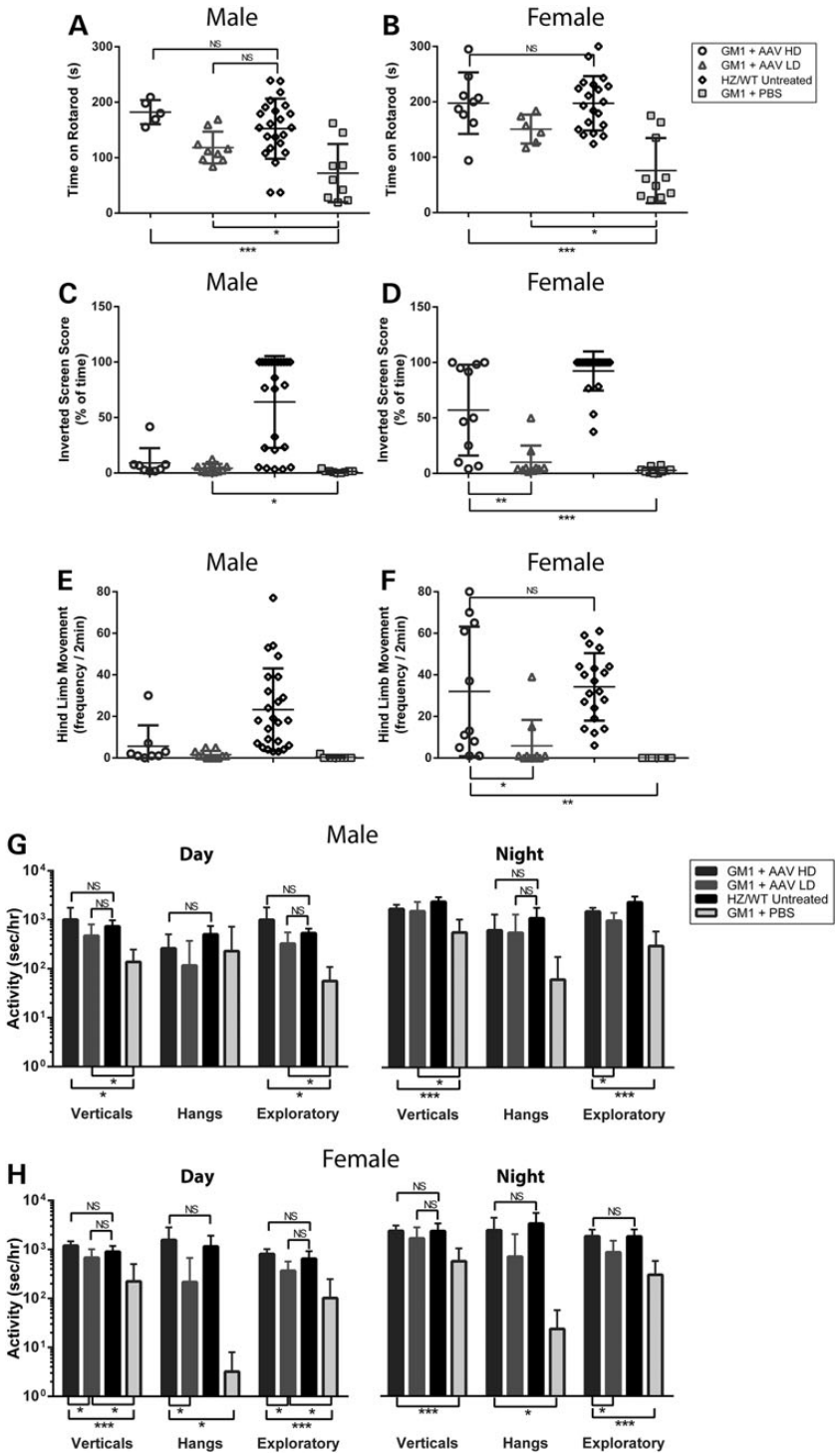

Figure 4. Improved behavioral performance of AAV9-treated GM1 mice. (**A** and **B**) Rotarod testing, (**C–F**) inverted screen testing or (**G** and **H**) home cage testing was carried out at 30 weeks of age for both LD (1×10^{11} vg) and HD (3×10^{11} vg) cohorts of AAV9-βgal-treated male and female GM1 mice (GM1 + AAV), normal HZ and WT animals, and PBS-treated GM1 mice (GM1 + PBS) at 30 weeks of age. (A and B) Rotarod testing—highest time achieved on a 4–40 rpm accelerating rotarod over 300 s over three trials. (C–F) Inverted screen testing—(C and D) inverted screen score, percentage of time on screen up to 120 s and (E and F) number of hind leg movements during this time. Second scoring of two trials reported. (A–F) Symbols indicate performance of one animal, error bars represent standard deviation ($N = 5–25$ animals/group). (G and H) Home cage testing—behaviors collected per second, tabulated per hour, averaged per animal and consolidated to represent a 10 h period of day or night assessed at ~37 weeks of age. The amount of daytime activity (left graphs) and nighttime activity (right graphs) spent on vertical movements (verticals), hangs and exploratory behaviors were assessed by time spent reaching, hanging and moving around the cage, respectively. Results are shown as mean ± SD. $N = 5–7$ per group. $^{*}P < 0.05$, $^{**}P < 0.01$ and $^{***}P < 0.001$, unpaired Student's *t*-test. NS indicates non-significant differences.

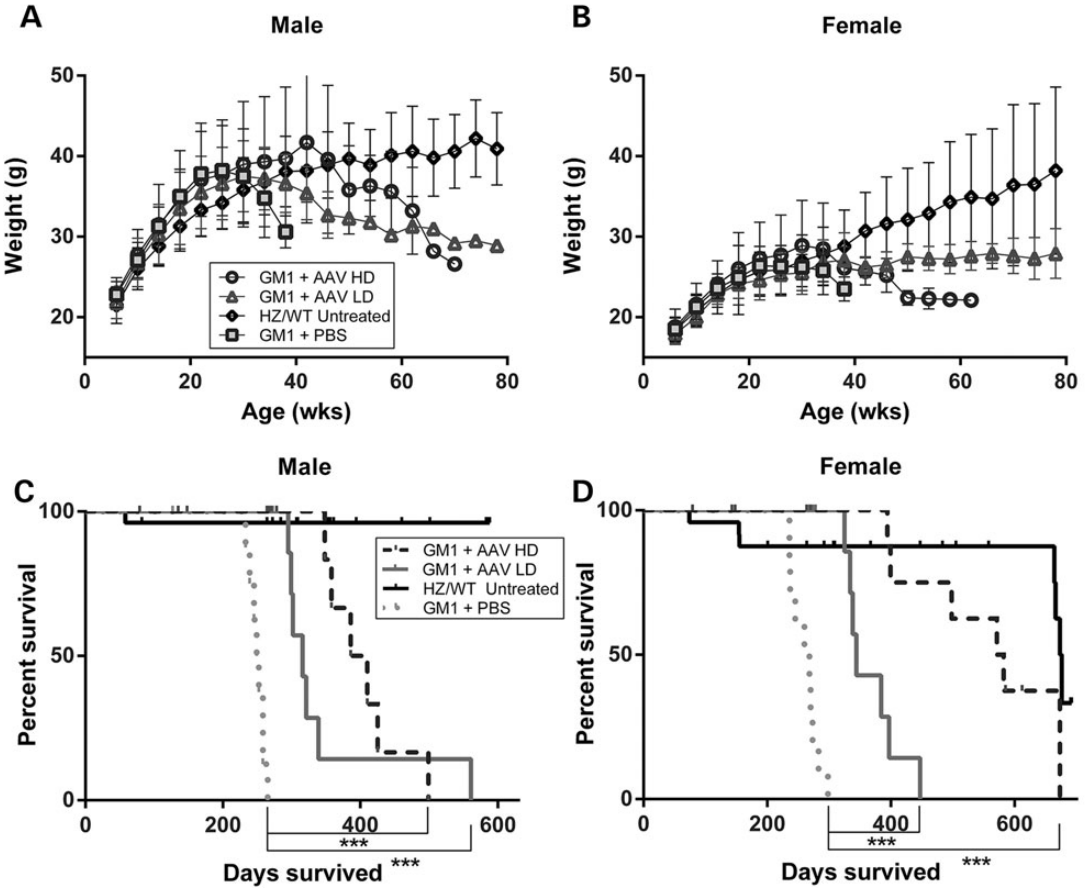

Figure 5. Survival of GM1 mice is increased by AAV9 treatment. (**A** and **B**) Body weight and (**C** and **D**) survival is shown for male and female AAV9-treated GM1 mice (GM1 + AAV) in the LD (1×10^{11} vg) and HD (3×10^{11} vg) cohorts, normal HZ or WT mice and PBS-treated GM1 mice (GM1 + PBS). Body weights are shown as mean ± SD. For survival analysis $N = 6$–10 per group. ***$P < 0.0003$, log-rank (Mantel–Cox) test.

Table 2. Weight and survival statistics of GM1 + AAV-treated mice and controls

Weight and survival statistics of GM1 + AAV-treated mice					
Gender	Genotype	Treatment	Age at max weight (days)	Median survival (days)	Max survival (days)
Male	HZ/WT	Untreated	513.8 ± 10.5	N/A	N/A
Male	GM1	PBS	178.5 ± 23.1	250.5	265
Male	GM1	1×10^{11} vg	245.7 ± 53.2**	316.0**	339[a]
Male	GM1	3×10^{11} vg	278.6 ± 61.6**	398.0***	499
Female	HZ/WT	Untreated	510.3 ± 42.0	N/A	N/A
Female	GM1	PBS	179.2 ± 24.5	264.0	298
Female	GM1	1×10^{11} vg	230.3 ± 38.5**	344.0***	447
Female	GM1	3×10^{11} vg	458.5 ± 76.3**	576.5***	673

[a]One animal survived until 561 days.
For age at max weight **$P < 0.01$ and ***$P < 0.001$, unpaired Student's t-test.
Significant difference for median survival of GM1 + AAV versus GM1 + PBS was determined using log-rank (Mantel–Cox) test where ***$P < 0.0003$.

controls ($P < 0.01$; Fig. 5 and Table 2). Survival analysis showed a significant increase in median survival for both genders and doses ($P < 0.0003$) compared with PBS-treated GM1 mice (Fig. 5C and D and Table 2). In addition, there was a significant difference in survival between doses for females ($P = 0.0007$), and between males and females in the HD cohort ($P = 0.01$) (Fig. 5C and D and Table 2).

Discussion

Previous studies from our lab have shown intracranial delivery of recombinant AAV vectors in neonatal (9) and adult GM1 mice (7) to be effective approaches to achieve widespread expression of functional βgal and reduce lysosomal storage of GM1-ganglioside in the CNS. The intracranial AAV delivery approach in adult GM1 mice delayed the onset of disease symptoms, but had little to no impact on the decline of motor function and only a modest improvement in survival (7).

In this study, we show that vascular delivery of a single-stranded AAV9 vector in adult GM1 mice extended survival (Fig. 5C and D and Table 2), but was not successful in arresting disease progression at the doses tested (1×10^{11} and 3×10^{11} vg/mouse). The therapeutic impact was considerably better in females with a median survival in the HD cohort of 576.5 days compared with 398.0 days for males (Fig. 5C and D and Table 2). The therapeutic outcomes correlate well with biochemical and histological findings in CNS where we observed increased βgal activity (Fig. 1; Supplementary Material, Table S1) and partial correction of GM1-ganglioside content (Fig. 2).

Histological analysis of lysosomal storage revealed dramatic reduction in the HD cohort cerebral cortex, hippocampus,

brainstem and spinal cord, but lesser impact in deep brain structures such as thalamus, and striatum, and importantly in the cerebellum (Fig. 2A and B). The reduction in lysosomal storage observed in thalamus, brainstem and spinal cord likely contributed to slower disease progression as the onset of symptoms in GM1 mice coincides with the detection of inflammatory markers in those structures (33). Despite partial correction in several CNS regions, the impact of AAV9 treatment on disease physiology was nonetheless profound in the HD cohort as indicated by the dramatic reduction in reactive astrocytes throughout the brain (Fig. 3A) that correlated with reduction in lysosomal storage (Fig. 2A and C). The therapeutic impact in the spinal cord with normalization of GM1-ganglioside content (Fig. 2B and C) and resolution of astrogliosis (Fig. 3B) was likely a major factor in extending the lifespan and preserving ambulation of AAV9-treated animals (Supplementary Material, Movies S1 and S2, S5 and S6). Nonetheless, AAV9-treated animals eventually developed whole body tremors and jerky movements, which may be related to the marginal therapeutic impact in the cerebellum (Supplementary Material, Movies S5–S6). AAV9-HD cohort—treated animals showed little or no change in lysosomal storage in granule and Purkinje cell layers, but complete correction in DCN (Fig. 2A–F, m thin and thick arrows, respectively). The failure to resolve storage in the Purkinje cell layer was also reported in another study using systemic delivery of an AAV9 vector to treat MPS IIIB mice (30). As the output centers of the cerebellum, the DCN send projections to different levels of the spinal cord and other regions of the brain (37). Given the connectivity of those nuclei and that βgal can be distributed over long distances via axonal transport (12), storage correction in DCN is most likely the result of enzyme uptake at axonal terminals in successfully treated structures, such as the spinal cord, and its retrograde transport to the cell body where most lysosomes reside. Disease progression in other cerebellar nuclei or cell populations may have led to the phenotypes that developed over time in AAV9-treated GM1 mice.

The pattern of lysosomal storage correction in the CNS of GM1 mice in this study matches closely results from other studies assessing the CNS transduction profile of AAV9 vectors delivered systemically in adult mice. The most effectively transduced CNS regions are the cerebral cortex, hippocampus and spinal cord (25, 38). Neuronal transduction in adult mice seems to be most pronounced in the spinal cord and hippocampus, but mostly glia and endothelial transduction throughout the rest of the brain (25,38). Transduction of striatum and thalamus appears relatively inefficient by comparison with other brain regions, and especially inefficient in cerebellum at comparable doses (38). Nonetheless, previous studies have reported exceptional therapeutic effects using systemic delivery of single-stranded AAV9 vectors in mouse models of MPS IIIA (29) and IIIB (30). The difference in therapeutic outcomes may be related to rates of disease progression specific to each LSD or mouse model. Alternatively, the outcomes in this study may be related to lower CNS gene transfer efficiency as suggested by lower vector genome content compared with a previous study employing the same dose of AAV9 vector (30) despite comparable levels in liver. The AAV9-mβgal vector biodistribution was comparable in age-matched GM1 ($\beta gal^{-/-}$) and normal ($\beta gal^{+/+}$) littermates as well as in C57BL6/J mice, suggesting that other variables may have determined the CNS gene transfer efficiency in this study. As an example, a previous study showed the CNS transduction profile of different AAV capsids to be influenced greatly by the purification method (39). Other aspects such as the minimum level of enzyme necessary to achieve complete correction of storage in cross-corrected cells may be considerably higher for βgal compared with other lysosomal enzymes. During synthesis βgal forms a megacomplex with neuraminidase-1 (NEU1) and protective protein/cathepsin A (PPCA), which is important for transport of NEU1 to lysosomes as well as processing/protection of βgal (reviewed in 40). Since only βgal is overexpressed, secreted and transported into enzyme-deficient cells, it is possible that its half-life may be lower in the lysosomes of cross-corrected cells because it may not interact with PPCA as the βgal-PPCA complex is normally formed before transport to lysosomes (40). This may render the recombinant βgal more susceptible to proteolytic degradation. In addition, the enzymatic efficiency of βgal by itself may be lower than in its native multienzyme complex. AAV vector design and dosing may also explain the difference in outcomes between our study and others.

The difference in therapeutic impact between genders is likely the result of a difference in CNS gene transfer efficiency as suggested by vector genome content (Table 1). Although the difference between genders did not reach statistical significance in most tissues, it is interesting that the average value is 2- to 3-fold higher in females across all brain regions ($P = 0.07$ for cerebrum and cerebellum) and in most other organs except liver and muscle (Table 1). The higher efficiency of AAV9 liver gene transfer in male mice has been documented in multiple models (41,42) and appears to be testosterone dependent (42). Our results show the same gender difference in AAV9 liver gene transfer with a 5-fold higher vector genome content (Table 1) and 6- to 7-fold higher enzyme activity in males than females in the HD cohort (Fig. 1B and C; Supplementary Material, Table S1). The notion that AAV9 CNS gene transfer after vascular delivery in adult GM1 mice is more efficient in females is supported by a recent study showing an identical gender difference in different mouse strains infused systemically with an AAV9 vector encoding firefly luciferase (43). The higher efficiency of AAV9 CNS gene transfer in females after systemic delivery may be partly due to lower affinity to liver. This suggests that liver tropism/affinity may be a major factor in determining the bioavailability of AAV9 (and possibly other AAV capsids) to transduce other organs after systemic delivery. The gender effect on AAV liver transduction has not been documented in other mammalian species such as cats. Nonetheless, liver tropism remains an important issue in the development of systemic AAV9 gene delivery approaches for neurological diseases. The liver tropism of AAV9 is a concern for vascular delivery approaches to treat neurological diseases as the high doses required to target CNS effectively could lead to collateral liver toxicity related to transgene expression. Transient liver toxicity may explain the paradoxical finding that the βgal activities in liver and serum were lower in mice (both sexes) receiving higher vector dose (Fig. 1B and C; Supplementary Material, Table S1). Further studies will be necessary to assess this possibility and uncover the causes, which could be related to βgal overexpression. Whether this is a finding unique to this enzyme or also applies to other lysosomal enzymes remains to be determined. Presently, we are unable to exclude the possibility that an immune response to AAV9 capsid and/or βgal could partly explain this paradoxical observation. However, immune responses in hemophilia patients infused with AAV2 encoding factor IX (44), or in Pompe mice infused with an AAV8 vector encoding human acid α-glucosidase under the ubiquitous CB promoter (45) resulted in either complete elimination or dramatic reduction in protein expression over time. Although we did not measure antibody titers to either AAV9 or βgal in serum, or cellular responses, indirect evidence suggests that an immune response may not be a major

determinant of liver βgal activity as it remained comparable between 37 weeks of age and humane endpoint (Supplementary Material, Fig. S1).

Different approaches have been employed to reduce or eliminate transgene expression in liver after vascular delivery of AAV9 vectors, namely using the CMV promoter that is downregulated over time (30), or incorporation of perfect miR-122 (highly expressed in liver) target sequences in the expression cassette 3′ untranslated region (46). These transcriptional detargeting approaches are likely to increase safety of vascular delivery of AAV9 vectors, but have no impact on its liver tropism properties. Interestingly, AAV9 mutants engineered to reduce liver tropism by more than 10-fold show only marginal increases in CNS gene transfer (47). Presently, the molecular basis for decreased liver tropism is unknown, namely whether the introduced mutations change the affinity to the same cell surface receptor or re-direct the capsid to another receptor entirely. Clearly, achieving higher CNS gene transfer with AAV9 vectors, or derivatives, is not as simple as reducing liver tropism. Other AAV capsids may display higher CNS gene transfer efficiency than AAV9 in adult mice, as recently shown for AAVrh8 (28).

The therapeutic outcome in this study is superior to that obtained by intracranial injection of an AAV1 vector into thalamus and DCN of adult GM1 mice (7). This finding is somewhat paradoxical as in the present study there was only partial correction of GM1-ganglioside content in the brain compared with complete normalization in the intracranial approach, while the findings are reversed in the spinal cord. This suggests that disease progression in the spinal cord may be an early driver of disease phenotypes in this mouse model, but ultimately partial treatment of other CNS regions will compromise survival. It is possible that treatment of adult GM1 mice with higher doses of AAV9 vector may lead to complete correction of lysosomal storage in the CNS and arrest disease progression completely. However, treatment with higher AAV9 vector doses represent a significant challenge for translation into patients as the production scales and cost increase dramatically. In addition, higher antigen burden increases the risk of triggering an immune response in patients, which may be addressed by short-term immune-suppression (48). An alternative to using higher doses of AAV9 may be using other AAV capsids that appear more efficient for CNS gene transfer after systemic delivery in adult mice (28). A recently initiated clinical trial with systemic infusion of an AAV9 vector in children afflicted with spinal muscular atrophy type I (ClinicalTrials.gov identifier NCT02122952) will provide invaluable safety information on this approach for treatment of neurodegenerative diseases.

This is the first study reporting on the therapeutic efficacy of vascular delivery of an AAV9 vector encoding βgal in adult GM1 mice. We showed successful widespread expression of functional enzyme throughout the CNS with resulting reduction in GM1-ganglioside storage and significant extension of lifespan with retention of motor function. To improve overall therapeutic outcomes, a focus on increasing enzyme delivered to the CNS is warranted as enzyme levels achieved in this study were insufficient to normalize GM1-ganglioside levels. This inability to normalize GM1-ganglioside content everywhere may have lead to an eventual inflammatory cascade resulting in loss of function in partially corrected regions. Intravascular infusion of AAV9 vector at higher doses, or using AAV capsids with higher CNS gene transfer efficiency (28), may result in complete biochemical correction of disease with normalization of phenotype and lifespan.

Materials and Methods

AAV vector design and production

The vector AAV-mβgal contains a two flanking AAV2 inverted terminal repeats, cytomegalovirus enhancer fused to a chicken β-actin promoter/rabbit β globin intron (49), cDNA of mouse lysosomal acid βgal and an SV40 poly A. Vector stock was produced by transient transfection of 293 cells and purified by CsCl gradient ultracentrifugation (UMass Medical School, Gene Therapy Center, Worcester, MA, USA).

Animal procedures

GM1-gangliosidosis (GM1) mice (35) were obtained originally from Dr. Kunihido Suzuki (Neuroscience Center, University of North Carolina, Chapel Hill, NC, USA). In our studies, the humane endpoint was defined by either paralysis of any limb or >15 weight loss % relative to the highest weight achieved for each animal. Six-week-old GM1 mice were injected with 200 µl of AAV9-βgal vector at 1×10^{11} or 3×10^{11} vg via the tail vein using a 27G insulin syringe (BD Biosciences, Franklin Lakes, NJ, USA). Mice were sacrificed by an overdose of ketamine/xylazine (Fort Dodge Animal Health, Fort Dodge, IA and Lloyd Laboratories, Inc., Shenandoah, IA, USA), cleared by transcardiac perfusion with ice cold PBS and harvested according to assay needs. One brain hemisphere and half a spinal cord was embedded in freezing medium, Neg 50 (Richard-Allan Scientific, Kalamazoo, MI, USA) and quickly frozen in a dry ice/2-methylbutane bath (ThermoFisher Scientific, Waltham, MA, USA). The remaining brain hemisphere was separated into cerebrum, cerebellum and brain stem, and, along with the second half of the spinal cord, frozen over dry ice and stored at –80°C. All other organs were frozen over dry ice or fixed in 4% paraformaldehyde in PBS (Sigma-Aldrich, St. Louis, MO, USA). All procedures were approved by the Institutional Animal Care and Use Committee at the University of Massachusetts Medical School, and performed in compliance with the NIH Guide for Care and Use of Laboratory Animals.

Histological analysis

Fresh frozen sagittal brain and transverse spinal cords sections were cut at 20 µm thickness on a cryostat (ThermoFisher Scientific) at –12/–13°C. βgal enzyme presence in brain and spinal cord sections was assessed by Xgal histochemical staining as described previously (9). GM1 storage was detected by Filipin staining as described previously (9).

βgal enzymatic assay

Tissues were homogenized and βgal activity (nmol/h/mg protein) was determined by reaction with 4-methylumberlliferyl-β-D-galactopyranoside (4-MU) (Sigma-Aldrich) in a 96-well plate format and normalized for protein content by Bradford assay (Bio-Rad, Waltham, MA, USA) as described previously (9).

Genome copy number

Tissue sections were extracted in a DNA clean environment and rinsed in sterile PBS. DNA was isolated using the DNeasy Blood and Tissue Kit (Qiagen, Valencia, CA, USA). Quantitative real-time polymerase chain reaction (PCR) was performed on 100–400 ng of genomic DNA using the following primers and probe to the SV40 polyA signal in the AAV vector: forward primer: AGCAA TAGCATCACAAATTTCACAA; reverse primer: CCAGACATGATAA

GATACATTGATGAGTT; probe: 6FAM-AGCATTTTTTTCACTGCAT TCTAGTTGTGGTTTGTC-TAMRA). Samples with genome copies ≥100 vg/μg of DNA were considered positive for vector genomes. Data was represented as vg/diploid genome considering that 100 ng of mouse genomic DNA corresponds to 13 889 diploid genomes (50).

GM1-ganglioside content

A liquid chromatography-tandem mass spectrometry (LC–MS/MS) method was used for quantification of GM1-ganglioside in CNS. Briefly, 0.01–0.04 mg/μl of tissue homogenate was diluted to 25 μl in buffer containing 0.2 M sodium acetate and 0.1 M NaCl (pH 4.3). To each sample, 3 μg of d_3-labeled GM1 (Matreya, LLC, Pleasant Gap, PA, USA) was added as an internal standard. Calibration curves were made neat with GM1-ganglioside (Avanti Polar Lipids, Alabaster, AL, USA) over the range of 200–3000 ng and spiked with 3000 ng of d_3-GM1. Total lipids were extracted by the Folch method (51) two successive times in chloroform/methanol (1 : 1), the supernatants combined, and the glycolipids partitioned to aqueous phase by adjusting the composition to chloroform/methanol/water (2 : 1 : 0.6). The upper aqueous phase was removed and the lower phase was washed once with chloroform/methanol/water (3 : 48 : 47) and the upper phases combined. Samples were dried, re-suspended in 0.2 ml 0.1 M NaCl and applied to an equilibrated 1 cc C18 reverse-phase Bond Elute column (Agilent Technologies, Santa Clara, CA, USA), washed with 5 ml water, eluted with 0.6 ml CH_3OH followed by 1 ml $CHCl_3 : CH_3OH$ (1 : 1), dried, and re-suspended in 100 μl solution of 1 : 4 (A : B) where A is 0.1% (v/v) formic acid and B is methanol : 2-propanol : 0.1% formic acid (47.5 : 47.5 : 4.9). Gangliosides were separated on a Phenomenex (Torrance, CA, USA) 2.1 × 50 mm Kinetex 1.7 μm (100 Å) C18 column using a Waters (Milford, MA, USA) Acquity UPLC using a fast gradient program (0–1 min, 80%B; 1–5 min, 80–100%B; 5–7 min 100%B; 7.1, 80% B) and eluted to a Waters Quattro Premier XE triple quadrupole mass spectrometer operating in the negative ion mode. Multiple reaction monitoring transitions for all GM1 species were monitored using a cone voltage of 90 V, a collision energy of 70 V and recorded the common sialic fragment anion at *m/z* 290. The area of all the individual GM1 lipid species (16 : 0, 18 : 0, 18 : 1, 20 : 0, 20 : 1) were combined for each ganglioside and the ratios were calculated to the corresponding d_3-18:0 GM1 internal standard. Calculated concentrations were normalized to protein content by Bradford (Bio-Rad).

Behavioral assays

Rotarod testing (52) was conducted on a Rotarod apparatus (Med Associates, St Albans, VT, USA) as follows. Animals were placed on an accelerating Rotarod from 4 to 40 rpm over 5 min and latency to fall recorded. Testing was conducted with one practice trial of 1 min accelerating from 2 to 20 rpm at the beginning of the session followed by three trials with 15–20 min resting in between. Latency to fall for each mouse in a testing session was recorded, and the longest time on the rotarod in any of the three trials was reported.

Inverted screen testing was performed on an apparatus as described previously (53). Animals were placed on a square wire mesh of 30 cm^2 with 25 mm^2 holes, over a cushioned surface. The screen was inverted slowly over a 2 s period, head over tail, until a 60° angle was reached and the screen then locked in place. Animals were assessed for latency to falling for up to 2 min and number of hind leg movements occurring during this time was also recorded. One practice trial and one testing run were administered to each mouse per time point with 15–20 min resting periods between trials.

Home cage testing was performed in an isolation cubicle (Med Associates), where mouse movement was tracked by video camera and processed by HomeCageScan software (CeleverSys, Reston, VA, USA) as described previously (34). Briefly, one animal was placed into the isolation cubicle in a clean cage identical to normal housing and containing food and water. The background area was subtracted in both light and dark conditions, and the animal's dimensions identified by the software. Data were taken regarding the animal's movement or inactivity and reported in seconds/behavior for a 26 h time period then collated according to behaviors.

Supplementary Material

Supplementary Material is available at *HMG* online.

Acknowledgments

We thank Art Allard (UMMS machine shop) for building behavioral testing rigs, and Karin Green (UMMS Proteomics and Mass Spectrometry Facility) for her assistance with the GM1-ganglioside analysis by LC–MS/MS. Finally, we thank Dr. Terry Flotte (UMass Medical School) for providing the AAV vector backbone.

Conflict of Interest statement. None declared.

Funding

This work was supported by the National Institutes of Health (R01HD060576 to M.S.E.).

References

1. Okada, S. and O'Brien, J.S. (1968) Generalized gangliosidosis, beta-galactosidase deficiency. *Science*, **160**, 1002–1004.
2. O'Brien, J.S., Stern, M.B., Landing, B.H., O'Brien, J.K. and Donnell, G.N. (1965) Generalized gangliosidosis, another inborn error of ganglioside metabolism? *Am. J. Dis. Child.*, **109**, 338–346.
3. Suzuki, K. (1968) Cerebral GM1-gangliosidosis, chemical pathology of visceral organs. *Science*, **159**, 1471–1472.
4. Brunetti-Pierri, N. and Scaglia, F. (2008) GM1 gangliosidosis, review of clinical, molecular, and therapeutic aspects. *Mol. Genet. Metab.*, **94**, 391–396.
5. Suzuki, Y., Oshima, A. and Nanba, E. (2008), *The Online Metabolic and Molecular Bases of Inherited Disease*. McGraw Hill, New York, pp. 1–101.
6. Takaura, N., Yagi, T., Maeda, M., Nanba, E., Oshima, A., Suzuki, Y., Yamano, T. and Tanaka, A. (2003) Attenuation of ganglioside GM1 accumulation in the brain of GM1 gangliosidosis mice by neonatal intravenous gene transfer. *Gene Ther.*, **10**, 1487–1493.
7. Baek, R.C., Broekman, M.L., Leroy, S.G., Tierney, L.A., Sandberg, M.A., d'Azzo, A., Seyfried, T.N. and Sena-Esteves, M. (2010) AAV-mediated gene delivery in adult GM1-gangliosidosis mice corrects lysosomal storage in CNS and improves survival. *PLoS ONE*, **5**, e13468–e13483.
8. McCurdy, V.J., Johnson, A.K., Gray-Edwards, H.L., Randle, A. N., Brunson, B.L., Morrison, N.E., Salibi, N., Johnson, J.A., Hwang, M., Beyers, R.J. *et al.* (2014) Sustained normalization

of neurological disease after intracranial gene therapy in a feline model. *Sci. Transl. Med.*, **6**, 231ra248.
9. Broekman, M.L., Baek, R.C., Comer, L.A., Fernandez, J.L., Seyfried, T.N. and Sena-Esteves, M. (2007) Complete correction of enzymatic deficiency and neurochemistry in the GM1-gangliosidosis mouse brain by neonatal adeno-associated virus-mediated gene delivery. *Mol. Ther.*, **15**, 30–37.
10. Sano, R., Tessitore, A., Ingrassia, A. and d'Azzo, A. (2005) Chemokine-induced recruitment of genetically modified bone marrow cells into the CNS of GM1-gangliosidosis mice corrects neuronal pathology. *Blood*, **106**, 2259–2268.
11. Passini, M.A., Lee, E.B., Heuer, G.G. and Wolfe, J.H. (2002) Distribution of a lysosomal enzyme in the adult brain by axonal transport and by cells of the rostral migratory stream. *J. Neurosci.*, **22**, 6437–6446.
12. Broekman, M.L., Tierney, L.A., Benn, C., Chawla, P., Cha, J.H. and Sena-Esteves, M. (2009) Mechanisms of distribution of mouse beta-galactosidase in the adult GM1-gangliosidosis brain. *Gene Ther.*, **16**, 303–308.
13. Hickman, S., Shapiro, L.J. and Neufeld, E.F. (1974) A recognition marker required for uptake of a lysosomal enzyme by cultured fibroblasts. *Biochem. Biophys. Res. Commun.*, **57**, 55–61.
14. Tardieu, M., Zerah, M., Husson, B., de Bournonville, S., Deiva, K., Adamsbaum, C., Vincent, F., Hocquemiller, M., Broissand, C., Furlan, V. *et al.* (2014) Intracerebral administration of adeno-associated viral vector serotype rh.10 carrying human SGSH and SUMF1 cDNAs in children with mucopolysaccharidosis type IIIA disease: results of a phase I/II trial. *Hum. Gene Ther.*, **25**, 506–516.
15. Hinderer, C., Bell, P., Gurda, B.L., Wang, Q., Louboutin, J.P., Zhu, Y., Bagel, J., O'Donnell, P., Sikora, T., Ruane, T. *et al.* (2014) Intrathecal gene therapy corrects CNS pathology in a feline model of mucopolysaccharidosis I. *Mol. Ther.*, **22**, 2018–2027.
16. Haurigot, V., Marco, S., Ribera, A., Garcia, M., Ruzo, A., Villacampa, P., Ayuso, E., Anor, S., Andaluz, A., Pineda, M. *et al.* (2013) Whole body correction of mucopolysaccharidosis IIIA by intracerebrospinal fluid gene therapy. *J. Clin. Invest.*, **123**, 3254–3271.
17. Cearley, C.N. and Wolfe, J.H. (2007) A single injection of an adeno-associated virus vector into nuclei with divergent connections results in widespread vector distribution in the brain and global correction of a neurogenetic disease. *J. Neurosci.*, **27**, 9928–9940.
18. Salegio, E.A., Samaranch, L., Kells, A.P., Mittermeyer, G., San Sebastian, W., Zhou, S., Beyer, J., Forsayeth, J. and Bankiewicz, K.S. (2013) Axonal transport of adeno-associated viral vectors is serotype-dependent. *Gene Ther.*, **20**, 348–352.
19. Cearley, C.N. and Wolfe, J.H. (2006) Transduction characteristics of adeno-associated virus vectors expressing cap serotypes 7, 8, 9, and Rh10 in the mouse brain. *Mol. Ther.*, **13**, 528–537.
20. Bosch, A., Perret, E., Desmaris, N. and Heard, J.M. (2000) Long-term and significant correction of brain lesions in adult mucopolysaccharidosis type VII mice using recombinant AAV vectors. *Mol. Ther.*, **1**, 63–70.
21. Skorupa, A.F., Fisher, K.J., Wilson, J.M., Parente, M.K. and Wolfe, J.H. (1999) Sustained production of beta-glucuronidase from localized sites after AAV vector gene transfer results in widespread distribution of enzyme and reversal of lysosomal storage lesions in a large volume of brain in mucopolysaccharidosis VII mice. *Exp. Neurol.*, **160**, 17–27.
22. Dodge, J.C., Clarke, J., Song, A., Bu, J., Yang, W., Taksir, T.V., Griffiths, D., Zhao, M.A., Schuchman, E.H., Cheng, S.H. *et al.* (2005) Gene transfer of human acid sphingomyelinase corrects neuropathology and motor deficits in a mouse model of Niemann-Pick type A disease. *Proc. Natl. Acad. Sci. USA*, **102**, 17822–17827.
23. Kaplitt, M.G., Feigin, A., Tang, C., Fitzsimons, H.L., Mattis, P., Lawlor, P.A., Bland, R.J., Young, D., Strybing, K., Eidelberg, D. *et al.* (2007) Safety and tolerability of gene therapy with an adeno-associated virus (AAV) borne GAD gene for Parkinson's disease: an open label, phase I trial. *Lancet*, **369**, 2097–2105.
24. Worgall, S., Sondhi, D., Hackett, N.R., Kosofsky, B., Kekatpure, M.V., Neyzi, N., Dyke, J.P., Ballon, D., Heier, L., Greenwald, B.M. *et al.* (2008) Treatment of late infantile neuronal ceroid lipofuscinosis by CNS administration of a serotype 2 adeno-associated virus expressing CLN2 cDNA. *Hum. Gene Ther.*, **19**, 463–474.
25. Foust, K.D., Nurre, E., Montgomery, C.L., Hernandez, A., Chan, C.M. and Kaspar, B.K. (2009) Intravascular AAV9 preferentially targets neonatal neurons and adult astrocytes. *Nat. Biotechnol.*, **27**, 59–65.
26. Bevan, A.K., Duque, S., Foust, K.D., Morales, P.R., Braun, L., Schmelzer, L., Chan, C.M., McCrate, M., Chicoine, L.G., Coley, B.D. *et al.* (2011) Systemic gene delivery in large species for targeting spinal cord, brain, and peripheral tissues for pediatric disorders. *Mol. Ther.*, **19**, 1971–1980.
27. Zhang, H., Yang, B., Mu, X., Ahmed, S.S., Su, Q., He, R., Wang, H., Mueller, C., Sena-Esteves, M., Brown, R. *et al.* (2011) Several rAAV vectors efficiently cross the blood-brain barrier and transduce neurons and astrocytes in the neonatal mouse central nervous system. *Mol. Ther.*, **19**, 1440–1448.
28. Yang, B., Li, S., Wang, H., Guo, Y., Gessler, D.J., Cao, C., Su, Q., Kramer, J., Zhong, L., Ahmed, S.S. *et al.* (2014) Global CNS transduction of adult mice by intravenously delivered rAAVrh.8 and rAAVrh.10 and nonhuman primates by rAAVrh.10. *Mol. Ther.*, **22**, 1299–1309.
29. Ruzo, A., Marco, S., Garcia, M., Villacampa, P., Ribera, A., Ayuso, E., Maggioni, L., Mingozzi, F., Haurigot, V. and Bosch, F. (2012) Correction of pathological accumulation of glycosaminoglycans in central nervous system and peripheral tissues of MPSIIIA mice through systemic AAV9 gene transfer. *Hum. Gene Ther.*, **23**, 1237–1246.
30. Fu, H., Dirosario, J., Killedar, S., Zaraspe, K. and McCarty, D.M. (2011) Correction of neurological disease of mucopolysaccharidosis IIIB in adult mice by rAAV9 trans-blood-brain barrier gene delivery. *Mol. Ther.*, **19**, 1025–1033.
31. Chen, Y.H., Clafin, K., Geoghegan, J.C. and Davidson, B.L. (2012) Sialic acid deposition impairs the utility of AAV9, but not peptide-modified AAVs for brain gene therapy in a mouse model of lysosomal storage disease. *Mol. Ther.*, **7**, 1393–1399.
32. Arthur, J.R., Heinecke, K.A. and Seyfried, T.N. (2011) Filipin recognizes both GM1 and cholesterol in GM1 gangliosidosis mouse brain. *J. Lipid Res.*, **52**, 1345–1351.
33. Jeyakumar, M., Thomas, R., Elliot-Smith, E., Smith, D.A., van der Spoel, A.C., d'Azzo, A., Perry, V.H., Butters, T.D., Dwek, R. A. and Platt, F.M. (2003) Central nervous system inflammation is a hallmark of pathogenesis in mouse models of GM1 and GM2 gangliosidosis. *Brain*, **126**, 974–987.
34. Steele, A.D., Jackson, W.S., King, O.D. and Lindquist, S. (2007) The power of automated high-resolution behavior analysis revealed by its application to mouse models of Huntington's and prion diseases. *Proc. Natl. Acad. Sci. USA*, **104**, 1983–1988.
35. Hahn, C.N., del Pilar Martin, M., Schroder, M., Vanier, M.T., Hara, Y., Suzuki, K., Suzuki, K. and d'Azzo, A. (1997)

Generalized CNS disease and massive GM1-ganglioside accumulation in mice defective in lysosomal acid beta-galactosidase. *Hum. Mol. Genet.*, **6**, 205–211.
36. Matsuda, J., Suzuki, O., Oshima, A., Ogura, A., Naiki, M. and Suzuki, Y. (1997) Neurological manifestations of knockout mice with beta-galactosidase deficiency. *Brain Dev.*, **19**, 19–20.
37. Dodge, J.C., Haidet, A.M., Yang, W., Passini, M.A., Hester, M., Clarke, J., Roskelley, E.M., Treleaven, C.M., Rizo, L., Martin, H. *et al.* (2008) Delivery of AAV-IGF-1 to the CNS extends survival in ALS mice through modification of aberrant glial cell activity. *Mol. Ther.*, **16**, 1056–1064.
38. Gray, S.J., Matagne, V., Bachaboina, L., Yadav, S., Ojeda, S.R. and Samulski, R.J. (2011) Preclinical differences of intravascular AAV9 delivery to neurons and glia: a comparative study of adult mice and nonhuman primates. *Mol. Ther.*, **19**, 1058–1069.
39. Klein, R.L., Dayton, R.D., Tatom, J.B., Henderson, K.M. and Henning, P.P. (2008) AAV8, 9, Rh10, Rh43 vector gene transfer in the rat brain: effects of serotype, promoter and purification method. *Mol. Ther.*, **16**, 89–96.
40. Bonten, E.J., Annunziata, I. and d'Azzo, A. (2014) Lysosomal multienzyme complex: pros and cons of working together. *Cell. Mol. Life Sci.*, **71**, 2017–2032.
41. Ruzo, A., Garcia, M., Ribera, A., Villacampa, P., Haurigot, V., Marco, S., Ayuso, E.A., Anguela, X.M., Roca, C., Agudo, J., Ramos, D. *et al.* (2012) Liver production of sulfamidase reverses peripheral and ameliorates CNS pathology in mucopolysaccharidosis IIIA mice. *Mol. Ther.*, **20**, 254–266.
42. Davidoff, A.M., Ng, C.Y.C., Zhou, J.F., Spence, Y. and Nathwani, A.C. (2003) Sex significantly influences transduction of murine liver by recombinant adeno-associated viral vectors through an androgen-dependent pathway. *Blood*, **102**, 480–488.
43. Maguire, C.A., Crommentyijn, M.H., Mu, D., Hudry, E., Serrano-Pozo, A., Hyman, B.T. and Tannos, B.A. (2013) Mouse gender influences brain transduction by intravascularly administered AAV9. *Mol. Ther.*, **21**, 1470–1471.
44. Manno, C.S., Pierce, G.F., Arruda, V.R., Glader, B., Ragni, M., Rasko, J.J., Ozelo, M.C., Hoots, K., Blatt, P., Konkle, B. *et al.* (2006) Successful transduction of liver in hemophilia by AAV-Factor IX and limitations imposed by the host immune response. *Nat. Med.*, **12**, 342–347.
45. Franco, L.M., Sun, B., Yang, X., Bird, A., Zhang, H., Schneider, A., Brown, T., Young, S.P., Clay, T.M., Amalfitano, A. *et al.* (2005) Evasion of immune responses to introduced human acid alpha-glucosidase by liver-restricted expression in glycogen storage disease type II. *Mol. Ther.*, **12**, 876–884.
46. Xie, J., Xie, Q., Zhang, H., Ameres, S.L., Hung, J.H., Su, Q., He, R., Mu, X., Seher Ahmed, S., Park, S. *et al.* (2011) MicroRNA-regulated, systemically delivered rAAV9: a step closer to CNS-restricted transgene expression. *Mol. Ther.*, **19**, 526–535.
47. Pulicherla, N., Shen, S., Yadav, S., Debbink, K., Govindasamy, L., Agbandje-McKenna, M. and Asokan, A. (2011) Engineering liver-detargeted AAV9 vectors for cardiac and musculoskeletal gene transfer. *Mol. Ther.*, **19**, 1070–1078.
48. Nathwani, A.C., Tuddenham, E.G., Rangarajan, S., Rosales, C., McIntosh, J., Linch, D.C., Chowdary, P., Riddell, A., Pie, A.J., Harrington, C. *et al.* (2011) Adenovirus-associated virus vector-mediated gene transfer in hemophilia B. *N. Engl. J. Med.*, **365**, 2357–2365.
49. Xu, L.F., Daly, T., Gao, C.H., Flotte, T.R., Song, S.H., Byrne, B.J., Sands, M.S. and Ponder, K.P. (2001) CMV-beta-actin promoter directs higher expression from an adeno-associated viral vector in the liver than the cytomegalovirus or elongation factor 1 alpha promoter and results in therapeutic levels of human factor X in mice. *Hum. Gene Ther.*, **12**, 563–573.
50. Hong, K.U., Li, Q.H., Guo, Y., Patton, N.S., Moktar, A., Bhatnagar, A. and Bolli, R. (2013) A highly sensitive and accurate method to quantify absolute numbers of c-kit+ cardiac stem cells following transplantation in mice. *Basic Res. Cardiol.*, **108**, 346–356.
51. Folch, J., Lees, M. and Sloane Stanley, G.H. (1957) A simple method for the isolation and purification of total lipides from animal tissues. *J. Biol. Chem.*, **226**, 497–509.
52. Qiu, L., Qiao, T., Beers, M., Tan, W., Wang, H., Yang, B. and Xu, Z. (2013) Widespread aggregation of mutant VAPB associated with ALS does not cause motor neuron degeneration or modulate mutant SOD1 aggregation and toxicity in mice. *Mol. Neurodegener.*, **8**, 1–16.
53. Jeyakumar, M., Butters, T.D., Cortina-Borja, M., Hunnam, V., Proia, R.L., Perry, V.H., Dwek, R.A. and Platt, F.M. (1999) Delayed symptom onset and increased life expectancy in Sandhoff disease mice treated with N-butyldeoxynojirimycin. *Proc. Natl. Acad. Sci. USA*, **96**, 6388–6393.